

MiniBooNE and LSND data: non-standard neutrino interactions in a (3+1) scheme versus (3+2) oscillations

Evgeny Akhmedov^{1,2,*} and Thomas Schwetz^{1,†}

¹*Max-Planck-Institut für Kernphysik,*

PO Box 103980, 69029 Heidelberg, Germany

²*National Research Center “Kurchatov Institute”*

123182 Moscow, Russia

Abstract

The recently observed event excess in MiniBooNE anti-neutrino data is in agreement with the LSND evidence for electron anti-neutrino appearance. We propose an explanation of these data in terms of a (3+1) scheme with a sterile neutrino including non-standard neutrino interactions (NSI) at neutrino production and detection. The interference between oscillations and NSI provides a source for CP violation which we use to reconcile different results from neutrino and anti-neutrino data. Our best fit results imply NSI at the level of a few percent relative to the standard weak interaction, in agreement with current bounds. We compare the quality of the NSI fit to the one obtained within the (3+1) and (3+2) pure oscillation frameworks. We also briefly comment on using NSI (in an effective two-flavour framework) to address a possible difference in neutrino and anti-neutrino results from the MINOS experiment.

*Electronic address: akhmedov@mpi-hd.mpg.de

†Electronic address: schwetz@mpi-hd.mpg.de

I. INTRODUCTION

Recently the MiniBooNE collaboration announced updated results of their search for $\bar{\nu}_\mu \rightarrow \bar{\nu}_e$ transitions [1]. In the full energy range from 200 MeV to 3 GeV they find an excess of 43.2 ± 22.5 events over expected background (the error includes statistical and systematical uncertainties). In the oscillation-sensitive region of 475 MeV to 1250 MeV the background-only-hypothesis has a probability of only 0.5% [1]. This result is consistent with the evidence for $\bar{\nu}_\mu \rightarrow \bar{\nu}_e$ transitions reported by LSND [2]. Any explanation of these hints for $\bar{\nu}_\mu \rightarrow \bar{\nu}_e$ transitions at the scale of $E/L \sim 1 \text{ eV}^2$ has to satisfy strong constraints from various experiments. First, no evidence for transitions has been found in MiniBooNE neutrino data above 475 MeV [3]. This suggests that CP (or even CPT) violation has to be invoked to reconcile neutrino and anti-neutrino data. Second, severe constraints exist for $\bar{\nu}_e$ [4, 5] and $\nu_\mu, \bar{\nu}_\mu$ [6–9] disappearance at this scale, which have to be respected by any explanation of the $\bar{\nu}_\mu \rightarrow \bar{\nu}_e$ excesses.

The standard approach to the LSND problem is to introduce one or more sterile neutrinos at the eV scale [10–12]. Adding one sterile neutrino one obtains the so-called (3+1) mass scheme. In this framework there is no CP violation at short baselines, and disappearance experiments strongly disfavour an explanation of the appearance signals, see for example [13, 14]. If two neutrino mass states at the eV scale are present [15, 16] ((3+2) scheme), the possibility of CP violation opens up [17], which allows to reconcile LSND and MiniBooNE neutrino data [18]. However, constraints from disappearance data still impose a challenge to the fit, and the overall improvement with respect to the (3+1) case is not significant [18, 19]. In the following we will update the (3+2) results of [18] with respect to the latest data from MiniBooNE anti-neutrinos.

Apart from sterile neutrino oscillations, various more exotic explanations of the LSND signal have been proposed, among them, neutrino decay [20, 21], CPT violation [13, 22–25], violation of Lorentz symmetry [26–28], quantum decoherence [29, 30], mass-varying neutrinos [31, 32], shortcuts of sterile neutrinos in extra dimensions [33] or sterile neutrino oscillations with a non-standard energy dependence [34].

In this work we attempt an explanation of the global data by departing from a (3+1) neutrino scheme through the inclusion of non-standard interactions (NSI) of neutrinos on top of the Standard Model weak interactions. Such new interactions may be induced by generic new physics beyond the Standard Model and can be neutral current (NC) like (involving only neutrinos in the lepton sector) or charged current (CC) like (involving a charged lepton and a neutrino). Model-independent bounds on such new interactions are at the level of $\text{few} \times 10^{-2}$ compared to the standard 4-Fermi interaction strength set by G_F , see [35] and references therein. An observation of NSI at that level would be a remarkable sign of new physics. The realization of NSI in terms of effective operators has been discussed recently in [36, 37].

Since the experiments considered here typically have rather short baselines (below 1 km),

matter effects are very small and NSI affecting the propagation of neutrinos through matter will have a negligible impact. Therefore, we focus on CC-like NSI in the production and detection processes, see for example [38–41]. As pointed out in [39], such NSI provide a new source of CP violation. Here we use this effect to reconcile neutrino and anti-neutrino data by exploring the interference of the NSI with sterile neutrino oscillations, with Δm^2 of order 1 eV². This allows us to keep NSI at the percent level. Previous attempts to explain the LSND excess by NSI without sterile neutrinos can be found in [42–44], while sterile neutrinos with an exotic matter effect have been considered in [45, 46].

In the following section II we derive an effective parameterisation of the transition and survival probabilities for short-baseline experiments, identifying the particular combinations of mixing and NSI parameters relevant for the experiments. We show that the probabilities for the global short-baseline data in a general (3+1) NSI model depend only on 8 independent parameters. In this case we can make use of the fact that in LSND and KARMEN the neutrino production mechanism is different from all other experiments. Therefore these experiments decouple to some extent from the rest of the global data. On the other hand, neglecting NSI involving the charged muon, only 5 independent parameters remain, which are only two independent parameters more than in the case of standard (3+1) oscillations, one modulus and one phase. In this case the fit is more constrained, while still providing significant improvement with respect to the pure oscillation case. As we will see, this constrained version requires only one single non-zero NSI parameter. In section III we present the results of global fits within these two versions of the (3+1) NSI model, the constrained 5 parameter version in section III A and the general one in III B. Furthermore, in section IV we present an updated fit in the (3+2) oscillation scheme and we compare the quality of the (3+1) NSI fits to the one of (3+2) oscillations. A summary and discussion follow in section V. In appendix A we relax some of the assumptions made on NSI parameters (showing that they do not change our results significantly), and in appendix B we comment briefly on using NSI to address a possible difference in neutrino and anti-neutrino results from the MINOS experiment [47].

II. NSI IN THE (3+1) MASS SCHEME

A. The formalism

We assume that, in addition to the standard charged current (CC) weak interactions, there exist non-standard CC-like interactions, whose Lagrangian can be parameterised at low energies as

$$\mathcal{L}_{\text{NSI}} = -2\sqrt{2}G_F \sum_{\alpha,\beta} \varepsilon_{\alpha\beta}^{ff'} (\bar{f} P_{L,R} \gamma^\mu f') (\bar{l}_\alpha P_L \gamma_\mu \nu_\beta) + h.c. . \quad (1)$$

Here G_F is the Fermi constant, f and f' correspond to either quarks or leptons differing by one unit of electric charge and l_α corresponds to a charged lepton ($l_\alpha = e, \mu, \tau$). $P_{L(R)}$

denotes the projection operator on left-handed (right-handed) fields. The particular chirality structure assumed in eq. (1) allows for interference of standard and non-standard processes. To simplify the notation we leave the dependence of ε on L/R implicit.

The interactions in eq. (1) contribute to CC processes of neutrino emission and absorption. In what follows, we will replace the superscript ff' by X ($X = S, D$), where $X = S$ stands for a concrete neutrino production process in the source and $X = D$ stands for the neutrino detection process. In the presence of NSI the neutrino state $|\nu_\alpha^X\rangle$ produced or detected in a CC process along with a charged lepton l_α is no longer the flavour eigenstate ν_α , but a linear combination of flavour eigenstates:

$$|\nu_\alpha^X\rangle = C_\alpha^X \left(|\nu_\alpha\rangle + \sum_\beta \varepsilon_{\alpha\beta}^X |\nu_\beta\rangle \right). \quad (2)$$

A similar relation holds for anti-neutrinos, with $\varepsilon_{\alpha\beta}^X$ replaced by $\varepsilon_{\alpha\beta}^{X*}$. Note that in our notation the first subscript at the parameter $\varepsilon_{\alpha\beta}^X$ always refers to the charged lepton and the second to the neutrino. C_α^X is a normalisation constant, which satisfies

$$|C_\alpha^X|^2 \left(1 + 2\text{Re} \varepsilon_{\alpha\alpha}^X + \sum_\rho |\varepsilon_{\alpha\rho}^X|^2 \right) = 1. \quad (3)$$

We also assume that, in addition to the standard three neutrino flavour states ν_e , ν_μ and ν_τ , there exists a fourth light neutrino, which necessarily has to be a sterile neutrino ν_s . As usual, the flavour states ν_e , ν_μ , ν_τ and ν_s are linear combinations of four mass eigenstates:¹

$$|\nu_\alpha\rangle = \sum_i U_{\alpha i}^* |\nu_i\rangle. \quad (4)$$

We assume that the 4th mass eigenstate is separated from the other three by a mass gap of order $\Delta m_{41}^2 \sim 1 \text{ eV}^2$ ((3+1) scheme). Alternatively, we will also consider a variant with two sterile neutrinos but no NSI ((3+2) scheme).

The state $|\nu_\alpha^X\rangle$ can also be expressed in terms of the mass eigenstates:

$$|\nu_\alpha^X\rangle = C_\alpha^X \sum_i \left(U_{\alpha i}^* + \sum_\beta \varepsilon_{\alpha\beta}^X U_{\beta i}^* \right) |\nu_i\rangle = C_\alpha^X \sum_{\beta, i} (\delta_{\alpha\beta} + \varepsilon_{\alpha\beta}^X) U_{\beta i}^* |\nu_i\rangle. \quad (5)$$

The probability amplitude for a neutrino ν_α^S born in a production process in the neutrino source to be detected as ν_β^D at a distance L from the source in a detection process is

$$\mathcal{A}_{\alpha\beta}(L) = \langle \nu_\beta^D | \nu_\alpha^S(L) \rangle = \sum_i F_{\alpha i}^S F_{\beta i}^{D*} e^{-iE_i L}, \quad (6)$$

¹ In the presence of NSI given in eq. (1), the usual flavour states can only be defined at the level of the Lagrangian, as the states coupled to the Standard Model W boson. Therefore, the mixing matrix U is the unitary matrix which diagonalises the neutrino mass matrix in the basis where the Standard Model CC interaction (without new physics contributions) is diagonal.

where E_i is the energy of the i th mass eigenstate neutrino and

$$F_{\alpha i}^X \equiv C_\alpha^X \sum_\rho (\delta_{\alpha\rho} + \varepsilon_{\alpha\rho}^X) U_{\rho i}^* . \quad (7)$$

Next, we note that for baselines and neutrino energies of interest, one can neglect all mass squared differences except those involving the fourth mass eigenstate. Denoting

$$\Delta \equiv \frac{\Delta m_{41}^2}{2E} L , \quad (8)$$

we can rewrite eq. (6) in the generic form

$$\mathcal{A}_{\alpha\beta}(L) = \alpha_{\alpha\beta}(e^{-i\Delta} - 1) + \beta_{\alpha\beta} , \quad (9)$$

where

$$\alpha_{\alpha\beta} = F_{\alpha 4}^S F_{\beta 4}^{D*} , \quad \beta_{\alpha\beta} = \sum_i F_{\alpha i}^S F_{\beta i}^{D*} . \quad (10)$$

The transition probability is then the squared modulus of the amplitude (9):

$$P_{\alpha\beta}(L) = 2 [|\alpha_{\alpha\beta}|^2 - \text{Re}(\beta_{\alpha\beta}^* \alpha_{\alpha\beta})] (1 - \cos \Delta) + |\beta_{\alpha\beta}|^2 + 2\text{Im}(\beta_{\alpha\beta}^* \alpha_{\alpha\beta}) \sin \Delta . \quad (11)$$

The probabilities for anti-neutrinos can be obtained from this formula by complex-conjugating the parameters $\alpha_{\alpha\beta}$ and $\beta_{\alpha\beta}$, i.e. by flipping the sign of the last term in eq. (11). Thus, in the presence of NSI the transition probabilities exhibit CP violation even in the one mass scale dominance limit, unlike in the case of pure oscillations. We will exploit this property of the considered model in order to reconcile the neutrino and anti-neutrino data in short-baseline appearance experiments. Since CP violation comes through the interference of $\alpha_{\alpha\beta}$ and $\beta_{\alpha\beta}$ terms it is important that both terms be present. It follows from eq. (11) that in order to suppress (enhance) the transition probability for neutrinos (anti-neutrinos) we need the phase of $\beta_{\alpha\beta}^* \alpha_{\alpha\beta}$ to be close to $3\pi/2$. Indeed, in our fits to be discussed in the following we will obtain numbers close to this value. Note that in general $P_{\alpha\beta}$ summed over either of the two indices will not give unity. This is because NSI break the unitarity of the neutrino evolution [48].

B. Application to short-baseline data

Let us now identify the effective parameters which are relevant for describing the short-baseline data used in our analysis, as summarised in tab. I, where we divide the experiments into appearance and disappearance searches.

1. Appearance experiments ($\mu \rightarrow e$). In this case we have

$$\alpha_{\mu e} = F_{\mu 4}^S F_{e 4}^{D*} , \quad (12)$$

Disappearance				Appearance			
Experiment	Ref.	Channel	Data	Experiment	Ref.	Channel	Data
Bugey	[4]	$\bar{\nu}_e \rightarrow \bar{\nu}_e$	60	LSND	[2]	$\bar{\nu}_\mu \rightarrow \bar{\nu}_e$	11
Chooz	[5]	$\bar{\nu}_e \rightarrow \bar{\nu}_e$	1	KARMEN	[49]	$\bar{\nu}_\mu \rightarrow \bar{\nu}_e$	9
Palo Verde	[50]	$\bar{\nu}_e \rightarrow \bar{\nu}_e$	1	NOMAD	[51]	$\nu_\mu \rightarrow \nu_e$	1
CDHS	[6]	$\nu_\mu \rightarrow \nu_\mu$	15	MiniB (ν)	[3]	$\nu_\mu \rightarrow \nu_e$	8
atmospheric	[18]	$\nu_\mu \rightarrow \nu_\mu$	1	MiniB ($\bar{\nu}$)	[1]	$\bar{\nu}_\mu \rightarrow \bar{\nu}_e$	8

TABLE I: Experiments used in the numerical analysis. The oscillation channel and the number of data points used in the fit (“Data”) are given. The total number of data points is 115.

where

$$\begin{aligned}
F_{\mu 4}^S &= C_\mu^S (U_{\mu 4}^* + \varepsilon_{\mu e}^S U_{e 4}^* + \varepsilon_{\mu \mu}^S U_{\mu 4}^* + \varepsilon_{\mu \tau}^S U_{\tau 4}^* + \varepsilon_{\mu s}^S U_{s 4}^*), \\
F_{e 4}^D &= C_e^D (U_{e 4}^* + \varepsilon_{ee}^D U_{e 4}^* + \varepsilon_{e \mu}^D U_{\mu 4}^* + \varepsilon_{e \tau}^D U_{\tau 4}^* + \varepsilon_{es}^D U_{s 4}^*).
\end{aligned}
\tag{13}$$

For the parameter $\beta_{\mu e}$ we obtain

$$\beta_{\mu e} = \sum_i F_{\mu i}^S F_{e i}^{D*} = C_\mu^S C_e^{D*} \left(\varepsilon_{\mu e}^S + \varepsilon_{e \mu}^{D*} + \sum_\rho \varepsilon_{\mu \rho}^S \varepsilon_{e \rho}^{D*} \right).
\tag{14}$$

In deriving this expression from eqs. (10) and (7) we have used unitarity of the leptonic mixing matrix. Notice that the transition probability $P_{\mu e}(L)$ does not vanish in the limit $L = 0$: in that case $P_{\mu e} = |\beta_{\mu e}|^2$. This is related to the fact that in the presence of NSI the states $|\nu_\mu^S\rangle$ and $|\nu_e^D\rangle$ are not orthogonal [52], see eq. (2). This should lead to a nontrivial signal in near detectors in appearance experiments.

2. Disappearance experiments. We will need the survival probabilities P_{ee} and $P_{\mu\mu}$. For the processes of interest (pion decay, nuclear beta decay and inverse beta processes), both neutrino production and detection involve transitions between u and d quarks. For the reactor experiments relevant for P_{ee} , production and detection are just inverse processes to each other. Therefore the relevant NSI are identical. For $P_{\mu\mu}$ the production process is pion decay, whereas detection proceeds via neutrino–nucleon capture. Since pions couple only to the axial current, vector-like NSI would not contribute to neutrino production but still show up in detection.² Hence, in this case it is possible that NSI at production and detection are different. We will discuss this possibility in appendix A. For the moment we simplify the discussion and assume that also for ν_μ disappearance NSI are identical in source and detection:

$$\varepsilon_{\mu\alpha}^S = \varepsilon_{\mu\alpha}^D \quad (\nu_\mu \text{ disappearance}).
\tag{15}$$

² We would like to thank Joachim Kopp for drawing our attention to this point.

This corresponds to axial-vector like NSI, $\varepsilon^{(A)} = \varepsilon^{(R)} - \varepsilon^{(L)}$. In this case we find from eqs. (10) and (3)

$$\alpha_{ee} \equiv \alpha_e = |F_{e4}^{ud}|^2, \quad \alpha_{\mu\mu} \equiv \alpha_\mu = |F_{\mu4}^{ud}|^2, \quad \beta_{ee} = \beta_{\mu\mu} = 1. \quad (16)$$

The equality of β_{ee} and $\beta_{\mu\mu}$ to unity is a reflection of the fact that at $L = 0$ the survival probabilities are equal to one. It should be stressed that this is only correct in the case when the neutrino production and detection processes are of the same type, i.e., $\varepsilon_{\alpha\beta}^S = \varepsilon_{\alpha\beta}^D$, as in the case we consider here. Otherwise the survival probabilities at $L = 0$ would be smaller than one. From eqs. (11) and (16) we find for the survival probabilities

$$P_{\beta\beta} = 1 - 2\alpha_\beta(1 - \alpha_\beta)(1 - \cos \Delta), \quad \beta = e, \mu. \quad (17)$$

There are no CP violation effects for the survival probabilities, again because we take $\varepsilon_{\alpha\beta}^S = \varepsilon_{\alpha\beta}^D$. Note that eq. (17) has the same structure as the disappearance probability for (3+1) oscillations with the identification $\alpha_\beta \rightarrow |U_{\beta4}|$, see e.g. [53].

In appendix A we will relax the assumption (15) and allow $\varepsilon_{\alpha\beta}^S \neq \varepsilon_{\alpha\beta}^D$ for ν_μ disappearance experiments. As we will discuss there, assuming $\varepsilon_{\alpha\beta}^S = \varepsilon_{\alpha\beta}^D$ has a small impact on the global fit and therefore we will adopt this simplification for our discussion apart from appendix A and where stated explicitly.

As mentioned above, for the disappearance experiments neutrino production and detection processes involve transitions between u and d quarks. This holds also for the Mini-BooNE and NOMAD appearance experiments. The only exceptions are LSND and KARMEN. While the detection process still involves u and d quarks (inverse beta decay), the production process is purely leptonic (muon decay)³, see also eqs. (A1) and (A2) in the appendix. Therefore, all experiments except LSND and KARMEN only depend on semi-leptonic NSI, and (under the assumption eq. (15)) we can drop the distinction between source and detector:

$$F_{\alpha i}^S = F_{\alpha i}^D \equiv F_{\alpha i}^{ud} \quad (\text{semi-leptonic NSI only}). \quad (18)$$

This means that the same NSI parameters appear for processes involving a given charged lepton α , irrespective of whether the process occurs at neutrino production or detection. If this relation holds, we obtain from eqs. (12) and (16) a factorisation property of the parameters α :

$$|\alpha_{\mu e}|^2 = \alpha_e \alpha_\mu. \quad (19)$$

³ We do not consider here the decay-in-flight data from LSND, where neutrinos are produced in pion decay. Muon decay contributes also to neutrino production in atmospheric neutrinos. We do not expect that this will have an important impact on our analysis and neglect this effect in the following, treating all NSI effects in atmospheric neutrinos as semi-leptonic.

Therefore, all experiments except LSND and KARMEN depend on the following set of parameters:

$$\alpha_e, \alpha_\mu, |\beta_{\mu e}|, \delta \equiv \text{Arg}(\alpha_{\mu e} \beta_{\mu e}^*), \Delta m_{41}^2. \quad (20)$$

For LSND and KARMEN purely leptonic NSI will also contribute, while semi-leptonic NSI involving the charged muon, $\varepsilon_{\mu\alpha}^{ud}$, will contribute to the other experiments but not to LSND and KARMEN. This leads effectively to a decoupling of these experiments from the others, and we can describe LSND and KARMEN by the three independent parameters

$$|\alpha_{\mu e}^{\text{LK}}|, |\beta_{\mu e}^{\text{LK}}|, \delta^{\text{LK}} \equiv \text{Arg}(\alpha_{\mu e}^{\text{LK}} \beta_{\mu e}^{\text{LK}*}) \quad (21)$$

in addition to the common Δm_{41}^2 . Note that in this framework MiniBooNE cannot be considered as a direct test of LSND, since due to the different production mechanisms different parameters enter the transition probabilities for the two experiments.

Therefore, the global data in the general (3+1) NSI scenario (under the assumption eq. (15)) depend on the 8 independent parameters shown in eqs. (20) and (21). We shall denote this case by NSI^g . In appendix A we relax the assumption eq. (15) and argue that the effect on the global fit is small. In addition to the general NSI^g case we will discuss in the following also a constrained scenario, denoted by NSI^c , which can be obtained by assuming that the relation (18) holds for the global data, also including LSND and KARMEN. This can be achieved by assuming that all NSI parameters involving the charged muon (leptonic as well as semi-leptonic) vanish:

$$\varepsilon_{\mu\beta}^X = 0. \quad (22)$$

In this case, we find from eq. (7) that $F_{\mu i}^S = F_{\mu i}^D = U_{\mu i}^*$ and eq. (18) holds for all experiments. Note that for the processes relevant to the experiments we consider we always have $F_{ei}^S = F_{ei}^D$, and if eq. (22) is fulfilled, also eq. (15) holds trivially. Then the global data depends only on the 5 parameters from eq. (20) and the factorisation (19) applies in general.

The factorisation (19) is analogous to the factorisation property that holds in the pure (3+1) oscillations case [53], and $4|\alpha_{\mu e}|^2$ can be identified with $\sin^2 2\theta_{\text{SBL}}$ in the limit $\beta_{\mu e} \rightarrow 0$, θ_{SBL} being an effective two-flavour mixing angle. Hence, for $\beta_{\mu e} = 0$ we recover the (3+1) oscillation case. The fact that the parameter $\alpha_{\mu e}$ of the appearance amplitude given in eq. (19) is a product of two quantities which are constrained to be small from disappearance data leads to the well-known tension between the LSND signal and disappearance data in (3+1) schemes. Including now NSI (still subject to the approximation (22)) we obtain two more independent parameters, namely $|\beta_{\mu e}|$ and the phase δ . Since $|\beta_{\mu e}|$ enters only in the appearance probability and is unconstrained by disappearance data, one might expect some improvement of the tension between these two data sets. We expect significant improvement of the fit in the NSI^g case, due to the decoupling of the LSND evidence from the rest of the global data.

In the following section III we will present the results of a fit to data in terms of the effective parameters given in eqs. (20) and (21). However in both cases, NSI^c and NSI^g , we will present also a specific realization in terms of the fundamental parameters $U_{\alpha 4}$ and $\varepsilon_{\alpha\beta}$.

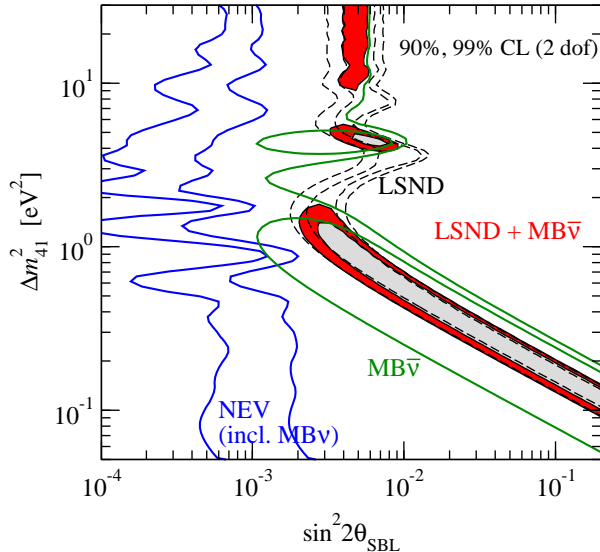


FIG. 1: Constraint from no-evidence data (NEV) compared to the combined allowed regions from LSND and MiniBooNE $\bar{\nu}$ data (shaded) at 90% and 99% CL for (3+1) oscillations. We show also the individual regions from LSND and MiniBooNE $\bar{\nu}$ data.

III. NUMERICAL RESULTS

In this section we present the results of fits to short-baseline data in the (3+1) NSI framework. The data used in the numerical analysis are summarised in tab. I. In total 115 data points are used. Technical details on our re-analysis of the experiments can be found in [18] and references therein. The constraint from atmospheric neutrino data is implemented in the following way. As discussed in detail in [18], atmospheric neutrinos provide a constraint on the parameter d_μ defined in that paper. d_μ corresponds to $|U_{\mu 4}|^2$ in the (3+1) oscillation case. Using the equivalence of the expressions for the survival probability in the (3+1) oscillation and (3+1) NSI schemes in eq. (17), we identify the parameters α_μ with d_μ from [18] and generalise the bound from atmospheric neutrinos now to hold for the parameter α_μ in the presence of NSI. A more accurate analysis of atmospheric neutrino data with NSI effects in source and detector is beyond the scope of this work. For the MiniBooNE anti-neutrino sample we fit the data shown in fig. 1 of [1], calibrating our prediction to the histogram shown in the lower part of that figure. As we will see later, in our model it is not possible to explain the low energy excess seen in MiniBooNE neutrino data (and to a lesser extent also in anti-neutrino data) below 475 MeV. Therefore, we follow the MiniBooNE collaboration and restrict the analysis to the oscillation-sensitive region above 475 MeV.

In fig. 1 we show our fit to MiniBooNE anti-neutrino data compared to the LSND region in the (3+1) oscillation framework without NSI. Our result is in good agreement with the

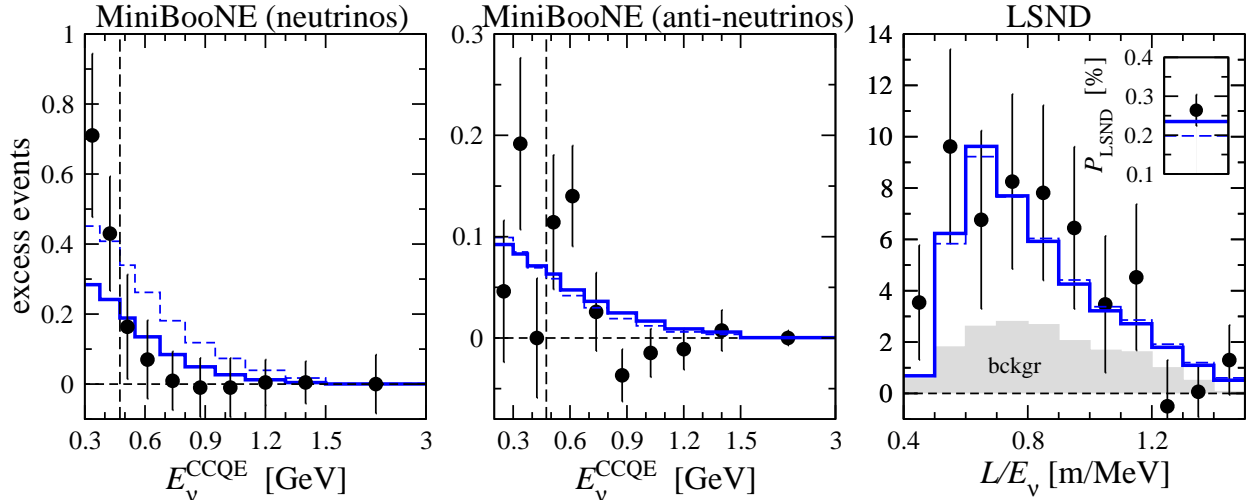


FIG. 2: Predicted event spectra at the best fit point to appearance data. Shown are the predictions for MiniBooNE neutrino (left), MiniBooNE anti-neutrino (middle), and LSND (right) compared to data. Dashed histograms refer to (3+1) oscillations, solid histograms to (3+1) NSI. The dashed vertical lines indicate the 475 MeV threshold used for MiniBooNE data. For LSND we show the spectrum with free normalisation and the value for the total transition probability (inset). The parameter and χ^2 values are given in tab. II.

region obtained in [1].⁴ We observe the overlap with the region indicated by LSND, which motivates the combined analysis of the two experiments shown as shaded regions. We also show the constraint coming from all the other experiments (“no-evidence” data, NEV), which excludes the region to the right of the blue curves. The figure shows the well known tension in the (3+1) oscillation fit: the regions touch each other at $\Delta\chi^2 = 12.7$, which corresponds to 99.8% CL for 2 dof.

A. The constrained (3+1) NSI model

Now we proceed to the (3+1) NSI model, starting with the constrained version NSI^c. As discussed in section II B, in this case the global data depends on the 5 parameters from eq. (20): α_e , α_μ , $|\beta_{\mu e}|$, δ , Δm_{41}^2 . For appearance data alone the parameters α_e and α_μ enter only in the combination $|\alpha_{\mu e}| \equiv \sqrt{\alpha_e \alpha_\mu}$, while disappearance data do not depend on $|\beta_{\mu e}|$ and δ . The limit of (3+1) oscillations is obtained for $|\beta_{\mu e}| = 0$.

First we consider appearance data only, i.e., MiniBooNE neutrino and anti-neutrino data, LSND, KARMEN, and NOMAD. The best fit parameters and χ^2 values are given in tab. II,

⁴ Differences can be attributed to the more sophisticated statistical analysis applied in [1], in contrast to the simple $\Delta\chi^2$ method based on the Gaussian approximation for 2 dof used here. In particular, Ref. [1] obtains a closed contour at 99% CL, while we find only a limit at 99% CL.

Data set	$ \alpha_{\mu e} $	$ \beta_{\mu e} $	δ	Δm_{41}^2	χ^2/dof
Appearance	0.2075	0.0091	1.5π	0.1 eV^2	$33.5/(37 - 4)$
Global	0.019	0.017	1.3π	0.89 eV^2	$107/(115 - 5)$

TABLE II: (3+1) NSI^c best fit parameter and χ^2 values for appearance data (LSND, MiniBooNE ν , MiniBooNE $\bar{\nu}$, KARMEN, NOMAD), and the global data. Corresponding event spectra are shown in figs. 2 and 3, respectively. For the global data we have $\alpha_e = 0.014$ and $\alpha_\mu = 0.026$ with $|\alpha_{\mu e}|^2 = \alpha_e \alpha_\mu$.

and fig. 2 shows the best fit spectra for MiniBooNE and LSND, where the dashed histograms correspond to (3+1) oscillations and solid histograms include NSI in addition. The figure illustrates the effect of CP violation: the best fit occurs at $\delta = 1.5\pi$ (maximal CP violation), and we observe the suppression of events for MiniBooNE neutrinos while maintaining the signal for anti-neutrinos in MiniBooNE and LSND. Let us mention that KARMEN and NOMAD provide an important constraint on the model, in particular they constrain $|\beta_{\mu e}|$ to be small. The $|\beta_{\mu e}|^2$ term in $P_{\mu e}$ corresponds to a pure NSI effect, independent of energy and distance, see eq. (11). Therefore the different value of L/E_ν of these experiments cannot be used to circumvent the bounds. This is one reason why a pure NSI explanation is very difficult, while in our model we can use the interference terms proportional to $\text{Re}(\alpha_{\mu e}\beta_{\mu e}^*)$ and $\text{Im}(\alpha_{\mu e}\beta_{\mu e}^*)$ in order to circumvent the constraint on the constant term. The relatively large value of $|\alpha_{\mu e}| \approx 0.2$ obtained in the fit is a consequence of the rather small Δm_{41}^2 , similar to the large mixing angle obtained for an oscillation fit of MiniBooNE anti-neutrino data only, see [1]. Such large amplitudes are excluded by disappearance data due to eq. (19), as we will see in the following.

The last row in tab. II gives the results of the global fit including all data, and the corresponding MiniBooNE and LSND spectra are shown in fig. 3. As mentioned above, disappearance data constrain $|\alpha_{\mu e}|$ to be small, and we now obtain $|\alpha_{\mu e}|$ and $|\beta_{\mu e}|$ of similar order, which maximises the CP effect. The phase δ is now slightly non-maximal, but fig. 3 still shows a relevant suppression of the events for MiniBooNE neutrino data, which contributes to the overall improvement of the fit. The constraint from disappearance data pushes the LSND transition probability to low values, and our best fit prediction $P_{\text{LSND}} = 0.19\%$ is about 1.8σ away from the measured value $P_{\text{LSND}}^{\text{exp}} = (0.264 \pm 0.04)\%$ (see inset of right panel in fig. 3).

In fig. 4 we show the allowed regions projected onto the plane of $|\alpha_{\mu e}|$ and $|\beta_{\mu e}|$ (left) as well as the $\Delta\chi^2$ as a function of $|\beta_{\mu e}|$ (right). The improvement of the fit compared to pure (3+1) oscillations ($|\beta_{\mu e}| = 0$) is

$$\chi_{\text{min},(3+1)\text{osc}}^2 - \chi_{\text{min},(3+1)\text{NSI}^c}^2 = 6.9 \quad (2 \text{ dof}), \quad (23)$$

where the number of dof corresponds to the two additional parameters of the (3+1) NSI^c model compared to (3+1) oscillations. Hence, the NSI case is favoured at 97% CL (slightly more than 2σ) compared to the pure oscillation case. From the right panel of fig. 4 we find

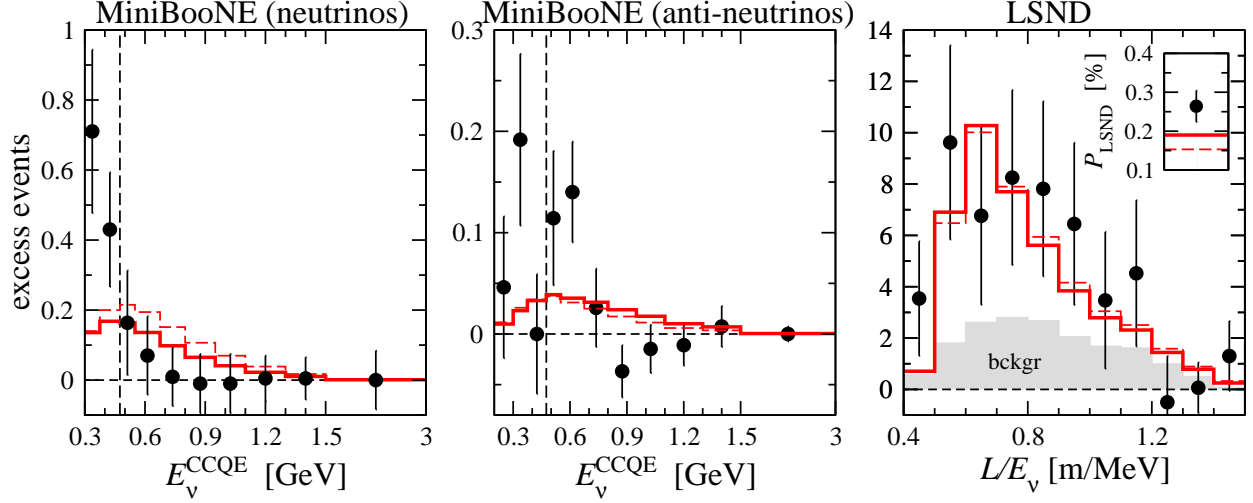


FIG. 3: Predicted event spectra at the best fit point to global data. Shown are predictions for MiniBooNE neutrino (left), MiniBooNE anti-neutrino (middle), and LSND (right) compared to data. Dashed histograms refer to (3+1) oscillations, solid histograms to (3+1) NSI^c. The dashed vertical lines indicate the 475 MeV threshold used for MiniBooNE data. For LSND we show the spectrum with free normalisation and the value for the total transition probability (inset). The parameter and χ^2 values are given in tab. II.

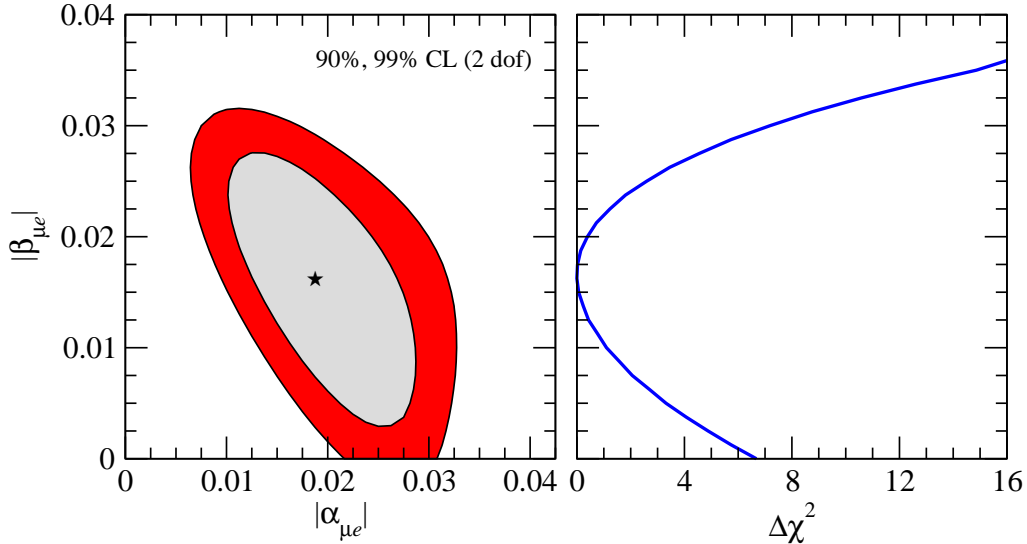


FIG. 4: Global fit in the (3+1) NSI^c framework. Left: allowed regions projected onto the plane of $|\alpha_{\mu e}|$ and $|\beta_{\mu e}|$ at 90% and 99% CL (2 dof). Right: $\Delta\chi^2$ as a function of $|\beta_{\mu e}|$. We minimise over all undisplayed parameters.

that the allowed interval for $|\beta_{\mu e}|$ (1 dof) does not include zero at the 2.6σ . We conclude that (3+1) NSI provides a significantly better fit than (3+1) oscillations. However, despite this relative improvement, we stress that some tension remains in the fit also for (3+1) NSI^c, as discussed below.

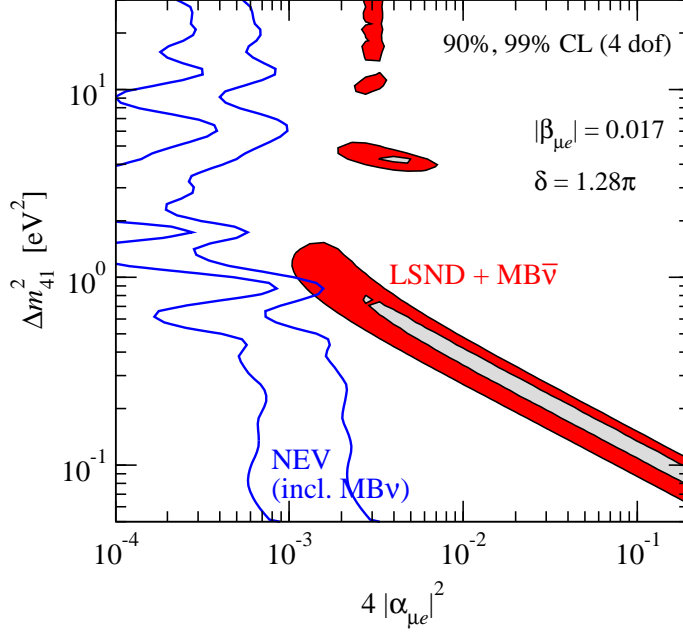


FIG. 5: Constraint from no-evidence data (NEV) compared to the combined allowed regions from LSND and MiniBooNE $\bar{\nu}$ data (shaded) at 90% and 99% CL for the (3+1) NSI^c case. The regions correspond to sections of the 4-dimensional allowed regions at fixed values of $|\beta_{\mu e}|$ and δ as given in the legend. These values correspond to the ones where the NEV constraint and the LSND+MB $\bar{\nu}$ allowed region touch each other (at $\Delta\chi^2 = 11.7$).

Fig. 5 shows the constraint from no-evidence experiments compared to the allowed region from LSND combined with MiniBooNE anti-neutrino data. This figure should be compared to fig. 1 for (3+1) oscillations. Note that the parameter $4|\alpha_{\mu e}|^2$ used in fig. 5 corresponds to the effective mixing angle $\sin^2 2\theta_{\text{SBL}}$ used in fig. 1 in the oscillation limit $|\beta_{\mu e}| \rightarrow 0$. The regions shown in fig. 5 are sections of the 4 dimensional volume (in the space $|\alpha_{\mu e}|, |\beta_{\mu e}|, \delta, \Delta m_{41}^2$) at the fixed values of $|\beta_{\mu e}|$ and δ for which the two regions start to touch each other. This happens at a $\Delta\chi^2 = 11.7$, corresponding to 98% CL for 4 dof. Therefore, we observe an overlap of the 99% CL regions. Clearly, while some tension remains in the fit, introducing NSI reduces the disagreement between evidence and no-evidence data.

Let us now address the question of how to realize the effective parameters from eq. (20) in terms of the fundamental parameters $U_{\alpha i}$ and $\varepsilon_{\alpha\beta}$ while respecting the phenomenological bounds. In fact, it is enough to assume only one single NSI parameter to be different from zero, namely $\varepsilon_{e\mu}^{ud}$. Then, we neglect the quadratic term in the normalisation factor C_e^X and the term containing the product of two small quantities, $\varepsilon_{e\mu}^{ud}$ and $U_{\mu 4}$, in the second equation in (13). As a result, we arrive at the following identification of the parameters relevant to our calculation:

$$\alpha_{\mu e} = U_{e4}U_{\mu 4}^*, \quad \beta_{\mu e} = \varepsilon_{e\mu}^{ud*}, \quad \alpha_e = |U_{e4}|^2, \quad \alpha_\mu = |U_{\mu 4}|^2. \quad (24)$$

From tab. II we obtain

$$|\varepsilon_{e\mu}^{ud}| \approx |\beta_{\mu e}| \approx 0.017 \quad (25)$$

at the global best fit point. This value is in safe agreement with the current bound on this parameter from CKM unitarity and lepton universality, which is of order 0.04 [35]. Note that the NOMAD experiment sets an even stronger bound of about 0.026 on this parameter. Since NOMAD data is explicitly included in the fit it is clear that our result respects even this stronger bound. While eq. (24) is just one simple example, we do not rule out here the possibility that other combinations of $U_{\beta 4}$ and $\varepsilon_{\alpha\beta}$ (including $\beta = s$ for the sterile neutrino) may lead to a similar fit.

One question that is still to be answered is if it is sufficient to have only one non-vanishing parameter $\varepsilon_{\alpha\beta}$ in order to have physically observable CP violation in neutrino transition probabilities. CP violation enters our formulas through the parameter $\text{Im}(U_{e4}U_{\mu 4}^*\varepsilon_{e\mu}^{ud})$. It is easy to see that the phase of the expression in the brackets cannot be rotated away by a rephasing of the involved fields, so that CP violation is physical in the case we consider.⁵

B. The general (3+1) NSI model

Let us now move to the general (3+1) NSI model (NSI^g), still assuming $\varepsilon^S = \varepsilon^D$ for ν_μ disappearance experiments, see eq. (15). As discussed in section II B, now LSND and KARMEN data are fitted by the new independent parameters $|\alpha_{\mu e}^{\text{LK}}|$, $|\beta_{\mu e}^{\text{LK}}|$, δ^{LK} , while all other experiments depend on a different set of parameters α_e , α_μ , $|\beta_{\mu e}|$, δ , where the factorisation $|\alpha_{\mu e}| = \sqrt{\alpha_e\alpha_\mu}$ holds. The only parameter in common between LSND/KARMEN and the rest is Δm_{41}^2 . Therefore, we have now 8 parameters in total.

In tab. III and fig. 6 we show the result of fits to appearance data only and global data. In the first case we obtain an excellent description of MiniBooNE and LSND data. We can invoke CP violation to reconcile MiniBooNE neutrino and anti-neutrino data, while maintaining an excellent fit to LSND data.⁶ However, in the second case, at the global best fit point, we observe from fig. 6 that the excess in MiniBooNE anti-neutrino data is not explained. The reason is that the constraint coming from MiniBooNE neutrino data

⁵ Indeed, U_{e4} can be made real, e.g., by rephasing ν_4 , and the phase of $U_{\mu 4}$ can be rotated away by rephasing μ . However, the parameter $\varepsilon_{e\mu}^{ud}$ cannot be made real after that because the phases of the e and ν_μ fields are already fixed. Note that a re-phasing of μ must be accompanied by the corresponding re-phasing of ν_μ due to the standard CC interaction term. One cannot eliminate the phase of $\varepsilon_{e\mu}^{ud}$ by rephasing the fields of u or d quarks that enter into eq. (1) because these fields enter similarly into both standard and non-standard interactions, and so the relative phase between these two kinds of terms is unaffected by rephasing u or d .

⁶ It turns out that allowing for NSI also leads to an improvement in the joint LSND + KARMEN fit. Due to the interference terms between $\alpha_{\mu e}^{\text{LK}}$ and $\beta_{\mu e}^{\text{LK}}$ there is more flexibility in the energy dependence of the transition probability, which improves the compatibility of the two experiments compared to a pure oscillation fit by several units in χ^2 .

Data set	$ \alpha_{\mu e}^{\text{LK}} $	$ \beta_{\mu e}^{\text{LK}} $	δ^{LK}	$ \alpha_{\mu e} $	$ \beta_{\mu e} $	δ	Δm_{41}^2	χ^2/dof
Appearance	0.31	0.029	0.49π	0.15	0.011	1.5π	0.13 eV^2	$29.4/(37-7)$
Global	0.053	0.036	0.39π	0.010	0.013	1.2π	0.89 eV^2	$95.4/(115-8)$

TABLE III: (3+1) NSI^g best fit parameter and χ^2 values for appearance data (LSND, MiniBooNE ν , MiniBooNE $\bar{\nu}$, KARMEN, NOMAD), and the global data. Corresponding event spectra are shown in figs. 6. For the global data we have $\alpha_e = 0.010$ and $\alpha_\mu = 0.011$ with $|\alpha_{\mu e}|^2 = \alpha_e \alpha_\mu$.

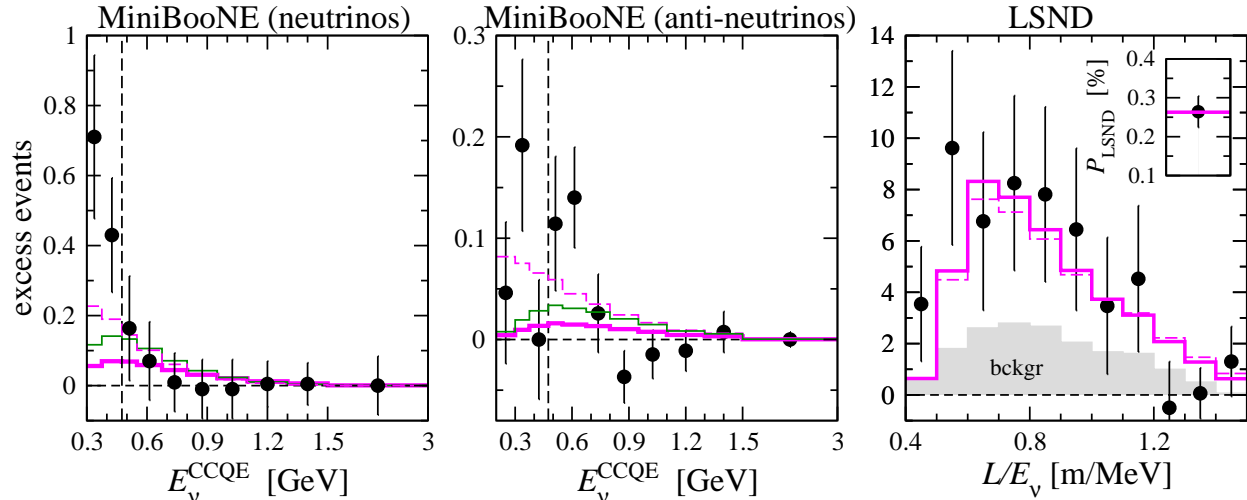


FIG. 6: Predicted event spectra at the (3+1) NSI^g best fit point to appearance data (dashed) and global data (thick-solid). Shown are predictions for MiniBooNE neutrino (left), MiniBooNE anti-neutrino (middle), and LSND (right) compared to data. The thin-solid (green) histograms for MiniBooNE show the global fit result without the assumption $\varepsilon^S = \varepsilon^D$ for ν_μ disappearance data (see appendix A). The dashed vertical lines indicate the 475 MeV threshold used for MiniBooNE data. For LSND we show the spectrum with free normalisation and the value for the total transition probability (inset). The corresponding parameter values are given in tab. III.

as well as from the disappearance experiments is much stronger than the positive signal in MiniBooNE anti-neutrino data. This is different in the NSI^c case (c.f., fig. 3), where the signal for MiniBooNE anti-neutrino data is directly linked to the LSND signal which is statistically much stronger. Let us mention that should the MiniBooNE anti-neutrino signal become more significant in the future, a mechanism similar to the one in the (3+1) NSI^c case (CP violation due to NSI) can be invoked to explain the excess while satisfying the bounds.

In the global fit we find a minimum χ^2 value of 95.4, which corresponds to

$$\chi_{\min,(3+1)\text{osc}}^2 - \chi_{\min,(3+1)\text{NSI}^g}^2 = 18.5 \quad (5 \text{ dof}), \quad (26)$$

where the number of dof corresponds to the additional 5 new parameters when extending the (3+1) oscillation scheme to NSI^g . The $\Delta\chi^2$ value corresponds to 99.76% CL. Hence,

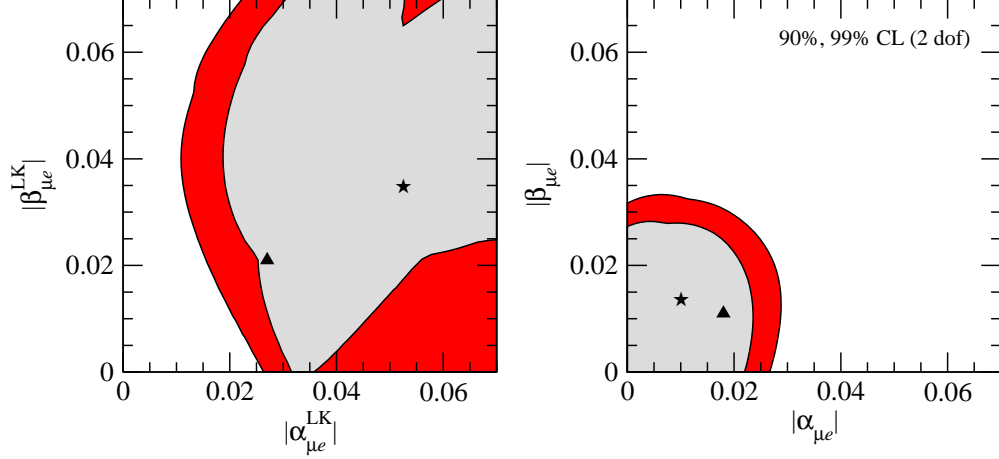


FIG. 7: Global fit in the (3+1) NSI^g framework. Left: allowed regions projected onto the plane of $\alpha_{\mu e}^{\text{LK}}$ and $\beta_{\mu e}^{\text{LK}}$ relevant for LSND and KARMEN, right: allowed regions projected onto the plane of $|\alpha_{\mu e}|$ and $|\beta_{\mu e}|$ relevant for all the other experiments. Regions are shown at 90% and 99% CL (2 dof). We minimise over all undisplayed parameters. The stars indicate the global best fit point, whereas the triangles correspond to the example from eq. (28).

(3+1) oscillation can be excluded at the 3σ level compared to the NSI^g case. In contrast to the NSI^c model, here the tension between appearance and disappearance experiments is significantly relaxed, since LSND (which provides the main appearance signal) is decoupled from the disappearance experiments. We will quantify this in the next section. Let us also mention that there is a nearly degenerate minimum to the one given in tab. III at $\Delta m_{41}^2 \approx 1.8 \text{ eV}^2$, see fig. 9 below.

We see from tab. III that the global NSI^g best fit point requires rather large values for the parameters $|\alpha_{\mu e}^{\text{LK}}|$ and $|\beta_{\mu e}^{\text{LK}}|$ relevant for LSND and KARMEN. However, the allowed regions shown in fig. 7 extend to rather small values even at the 90% CL. In the following we provide one possible realization in terms of fundamental mixing and NSI parameters. It turns out that the main difficulty in finding ε parameters within the present bounds is to obtain $|\alpha_{\mu e}^{\text{LK}}| \gtrsim 0.02$ while maintaining $|\alpha_{\mu e}| \lesssim 0.02$, compare with fig. 7.

Let us take the following ε to be non-zero:

$$|\varepsilon_{\mu s}^{ud}| \approx 0.05, \quad |\varepsilon_{e\mu}^{ud}| \approx 0.011, \quad |\varepsilon_{\mu s}^{e\nu}| \approx 0.03, \quad |\varepsilon_{\mu e}^{e\nu}| \approx 0.01. \quad (27)$$

Here the superscript $e\nu$ indicates the purely leptonic NSI relevant for the muon decay. These values are in agreement with the bounds derived in [35]. Using the fit results and eqs. (12),

(13), (14) we obtain

$$\begin{aligned}
|\alpha_{\mu e}| &\approx (|U_{\mu 4}| - |\varepsilon_{\mu s}^{ud}|)|U_{e 4}| \approx 0.018, \\
|U_{e 4}| &\approx 0.116, \quad |U_{\mu 4}| \approx 0.205, \\
|\beta_{\mu e}| &\approx |\varepsilon_{e\mu}^{ud}| \approx 0.011, \\
|\alpha_{\mu e}^{\text{LK}}| &\approx (|U_{\mu 4}| + |\varepsilon_{\mu s}^{e\nu}|)|U_{e 4}| \approx 0.027, \\
|\beta_{\mu e}^{\text{LK}}| &\approx |\varepsilon_{e\mu}^{ud}| + |\varepsilon_{\mu e}^{\nu e}| \approx 0.021.
\end{aligned} \tag{28}$$

Here we have assumed $|U_{s4}| \approx 1$ and neglected terms that are quadratic in small quantities. Note that we make use of the freedom to choose the phases of the ε to suppress $|\alpha_{\mu e}|$ and enhance $|\alpha_{\mu e}^{\text{LK}}|$. The χ^2 at this point (with $\Delta m_{41}^2 = 0.98 \text{ eV}^2$) is $\chi^2 = 101.0$, about 5.6 units larger than the best fit point from tab. III, obtained in the phenomenological analysis without taking into account constraints on NSI parameters. Considering that the model has 8 parameters, a $\Delta\chi^2 = 5.6$ corresponds to 69% CL. Therefore, the point from eq. (28) is located close to the 1σ volume in the 8-dimensional parameter space.⁷

Let us stress that this point is not optimised and should just serve as an example. Ideally a full analysis should be performed in terms of the fundamental parameters $U_{\alpha 4}$ and $\varepsilon_{\alpha\beta}$, taking into account the constraints on the latter. We leave such a fit for future work and proceed here with the phenomenological analysis in terms of the α and β parameters.

Let us comment now on the relevance of the assumption eq. (15), of equal NSI at production and detection for ν_μ disappearance experiments, which we so far have always adopted. This assumption can be relaxed by using the fact that vector-like NSI do not contribute to pion decay. As discussed in appendix A, this allows one to decouple the ν_μ disappearance data. The results of such a fit are shown as the thin-solid (green) histogram in fig. 6. We find that the predicted spectra for MiniBooNE are qualitatively very similar to our default NSI^g fit. We obtain at the best fit point $\chi^2 = 92.7$, to be compared with 95.4 for the standard NSI^g including the assumption eq. (15). Hence, the improvement of the fit by relaxing this assumption is not significant. The reason is that even with the assumption $\varepsilon^S = \varepsilon^D$ for ν_μ disappearance experiments, the constraints from CDHS and atmospheric data are satisfied in the global fit. Therefore, relaxing this assumption leads only to an insignificant improvement of the fit. Furthermore, as discussed in appendix A, this solution requires relatively large NSI parameters (of order 0.1) and cancellations between ε 's and elements of the mixing matrix. For these reasons we do not consider this possibility further and stick to the NSI^g scenario with the assumption eq. (15).

⁷ The value of $|\varepsilon_{\mu s}^{ud}|$ given in eq. (27) is somewhat large (though in agreement with the bounds from [35]).

It is used to partially cancel the value of $|U_{\mu 4}|$ in $|\alpha_{\mu e}|$. A solution with $|\varepsilon_{\mu s}^{ud}| = 0$ leads to a fit of similar quality with $\Delta\chi^2 \approx 7.7$.

	$ U_{e4}U_{\mu4} $	Δm_{41}^2	$ U_{e5}U_{\mu5} $	Δm_{51}^2	δ	χ^2/dof
Appearance	0.397	0.94 eV ²	0.375	1.0 eV ²	1.01 π	26.3/(37 - 5)
	$ U_{e4} $	$ U_{\mu4} $	$ U_{e5} $	$ U_{\mu5} $		
Global data	0.10	0.15	0.47 eV ²	0.13	0.17	0.89 eV ² 1.69 π 109/(115 - 7)

TABLE IV: Parameter and χ^2 values of the best fit points in the (3+2) oscillation scheme for appearance data from LSND, MiniBooNE ν and $\bar{\nu}$, KARMEN, NOMAD (upper part), and global data (lower part).

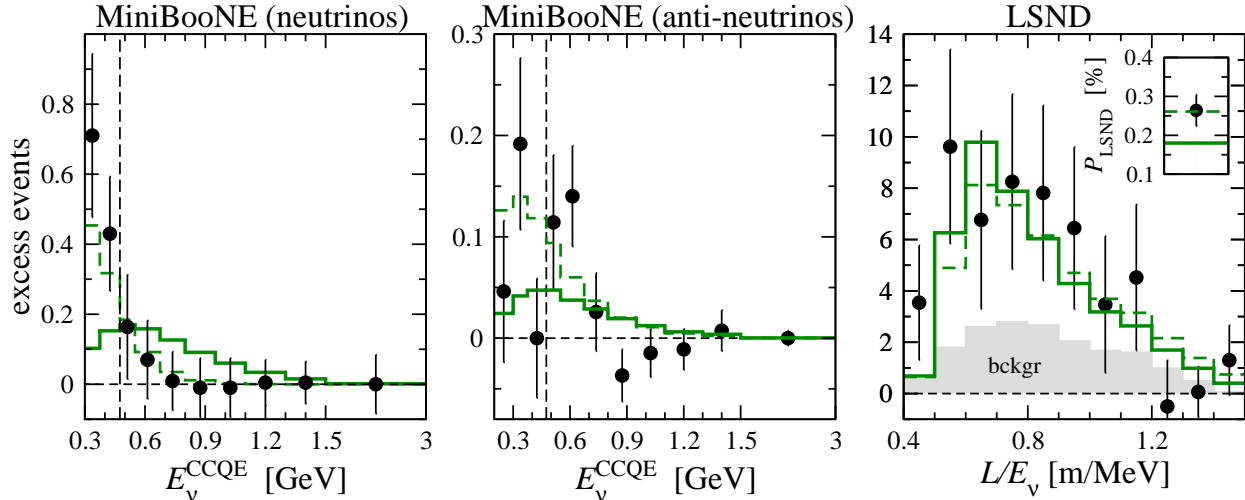


FIG. 8: Predicted event spectra at the (3+2) oscillation best fit point to appearance data (dashed) and global data (solid). Shown are predictions for MiniBooNE neutrino (left), MiniBooNE anti-neutrino (middle), and LSND (right) compared to data. The dashed vertical lines indicate the 475 MeV threshold used for MiniBooNE data. For LSND we show the spectrum with free normalisation and the value for the total transition probability (inset). The corresponding parameter values are given in tab. IV.

IV. COMPARISON OF (3+1) NSI WITH (3+2) OSCILLATIONS

In this section we present an update of the (3+2) oscillation analysis from [18] with respect to the anti-neutrino data from MiniBooNE. In this model appearance and global data depend on 5 and 7 parameters, respectively, as given in tab. IV. One physical complex phase allows for CP violation in $\nu_\mu \rightarrow \nu_e$ oscillations [17] and is given by

$$\delta \equiv \arg(U_{e4}^* U_{\mu4} U_{e5} U_{\mu5}^*) . \quad (29)$$

The best fit points for appearance and global data are given in tab. IV and the corresponding event spectra for MiniBooNE and LSND are shown in fig. 8. Considering appearance data only, a very good fit is obtained for neutrino and anti-neutrino data thanks to CP violation and even the MiniBooNE ν and $\bar{\nu}$ low energy data can be explained due to some cancellations between terms involving the two mass-squared differences and $\delta \approx \pi$, as discussed in [18]. However, rather large values of the amplitudes $|U_{e4}U_{\mu4}|$ and $|U_{e5}U_{\mu5}|$ are

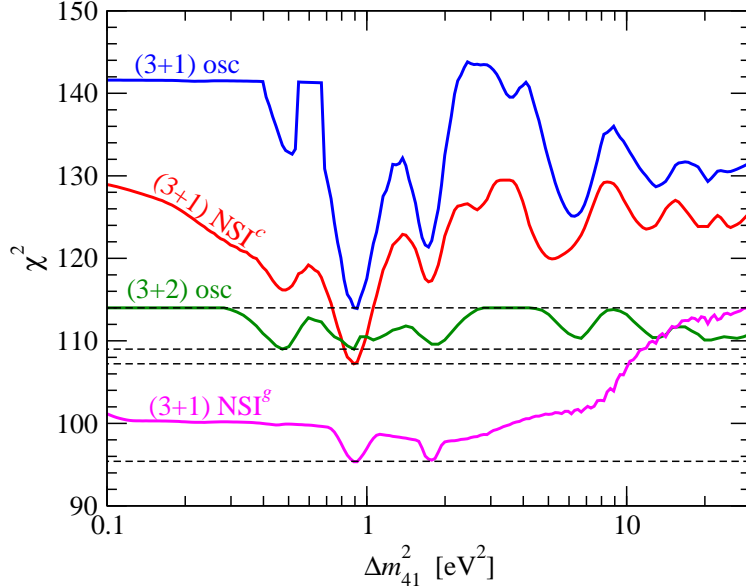


FIG. 9: χ^2 of global data as a function of Δm_{41}^2 for the (3+1) oscillation, (3+1) NSI^c, (3+1) NSI^g, and (3+2) oscillation models. In each case we minimise with respect to all parameters except Δm_{41}^2 . The horizontal dashed lines indicate the global minima.

needed, in disagreement with constraints from disappearance data.

In the global analysis some tension is visible in the spectra shown in fig. 8. The predicted event rate for MiniBooNE neutrino data is somewhat too high and the probability for LSND is somewhat low: $P_{\text{LSND}} = 0.18\%$, similar to the (3+1) NSI^c case. Furthermore, it is not possible to explain the low energy data in MiniBooNE below 475 MeV. The relative improvement of the fit due to introducing the second sterile neutrino is

$$\chi_{\min, (3+1)\text{osc}}^2 - \chi_{\min, (3+2)\text{osc}}^2 = 5.0 \quad (4 \text{ dof}), \quad (30)$$

where the number of dof corresponds to the additional 4 parameters introduced by moving from (3+1) to (3+2). The value given in eq. (30) corresponds to 71% CL, to be compared to 97% CL for NSI^c (eq. (23)) and 99.76% CL for NSI^g (eq. (26)). We conclude that both versions of the NSI model (but especially the unconstrained case) offer significantly more improvement of the global fit compared to the (3+2) oscillation scheme, when considering the χ^2 gain per new parameter. The previous (3+2) value obtained in [18] without MiniBooNE anti-neutrino data was 81% CL ($\Delta\chi^2 = 6.1$). Therefore, we find that the relative improvement of the fit when moving from (3+1) to (3+2) oscillations is smaller with the new global data than without MiniBooNE $\bar{\nu}$ data.

The χ^2 profiles as a function of Δm_{41}^2 for the four models—(3+1) oscillation, (3+1) NSI^c, (3+1) NSI^g, and (3+2) oscillation—are shown in fig. 9. In this plot we minimise with respect to all parameters except Δm_{41}^2 . Note that the maximal χ^2 for (3+2) is given by the χ^2 minimum in (3+1), since the (3+1) solution with Δm_{51}^2 is always available for any value of Δm_{41}^2 . Note also that there are two degenerate minima for (3+2) at $\Delta m_{41}^2 = 0.47 \text{ eV}^2$

	(3+1) NSI ^c		(3+1) NSI ^g		(3+2) oscillations	
	$\chi^2_{\text{PG}}/\text{dof}$	PG prob.	$\chi^2_{\text{PG}}/\text{dof}$	PG prob.	$\chi^2_{\text{PG}}/\text{dof}$	PG prob.
Evid. vs no-evid.	23.3/4	1.1×10^{-4}			26.9/5	6×10^{-5}
Appear. vs disapp.	11.5/2	3×10^{-3}	3.8/2	15%	21.7/4	2.3×10^{-4}
	$\Delta\chi^2/\text{dof}$	CL	$\Delta\chi^2/\text{dof}$	CL	$\Delta\chi^2/\text{dof}$	CL
Fit wrt (3+1) osc.	6.9/2	97%	18.5/5	99.76%	5.0/4	71%

TABLE V: Comparison of (3+1) NSI and (3+2) oscillations. We show the compatibility of LSND + MiniBooNE anti-neutrino data (“Evid.”) compared to the rest of the global data (“no-evid.”), and the appearance versus disappearance experiments. χ^2_{PG} , number of dof, and the corresponding probability are given. The lower part of the table shows the improvement with respect to the (3+1) pure oscillation case. We give the improvement in χ^2 , where the dof corresponds to the number of additional parameters.

and 0.89 eV² corresponding just to a relabeling of the mass-squared differences, compare with tab. IV. The relative improvement of the three models NSI^c, NSI^g, and (3+2) with respect to the (3+1) oscillation case is summarised in the lower part of tab. V.

Further insight in the quality of the fit can be obtained by evaluating the compatibility of different data sets with the so-called parameter goodness-of-fit (PG) [54]. It is based on the χ^2 function $\chi^2_{\text{PG}} = \chi^2_{\text{tot,min}} - \sum_i \chi^2_{i,\text{min}}$, where $\chi^2_{\text{tot,min}}$ is the χ^2 minimum of all data sets combined and $\chi^2_{i,\text{min}}$ is the minimum of the data set i . This χ^2 function measures the “price” one has to pay by the combination of the data sets compared to fitting them independently. It should be evaluated for the number of dof corresponding to the number of parameters in common to the data sets, see [54] for a precise definition.

In tab. V we show the results of such an analysis, testing the compatibility of evidence versus no-evidence data (similar as shown in fig. 5) and appearance versus disappearance data. These results indicate that in (3+2) as well as in (3+1) NSI^c significant tension remains between various data sets. For the general NSI model NSI^g, however, we find excellent agreement between appearance and disappearance data. In this case LSND is decoupled from the disappearance experiments and this tension is completely resolved. The evidence in MiniBooNE anti-neutrino data is not strong enough yet to show up as significant tension in the PG test. We do not perform the evidence versus no-evidence test for NSI^g, since it makes no sense to add LSND and MiniBooNE anti-neutrino data here because, as we have seen in fig. 6, the MiniBooNE $\bar{\nu}$ excess is not explained in the global fit in this model.

V. SUMMARY AND DISCUSSION

Recent MiniBooNE anti-neutrino data indicate an excess of $\bar{\nu}_e$ events, in agreement with the LSND evidence for $\bar{\nu}_\mu \rightarrow \bar{\nu}_e$ transitions. It is known that oscillations with a single sterile neutrino at the eV scale are not sufficient to explain the global data. We have investigated

the possibility that in addition to a sterile neutrino there are some non-standard neutrino interactions (NSI), beyond the Standard Model weak interactions. Since matter effects are tiny for the short baselines relevant here, we considered charged-current type NSI in the neutrino source and detector, parametrised by $\varepsilon_{\alpha\beta}$ as defined in eq. (1). Thanks to the interference between NSI effects and oscillations with $\Delta m_{41}^2 \sim 1 \text{ eV}^2$ we obtain CP violation, even in the presence of only one mass scale. This effect is used to reconcile the indication for $\bar{\nu}_\mu \rightarrow \bar{\nu}_e$ in anti-neutrino experiments (LSND and MiniBooNE) with the absence of a signal in MiniBooNE neutrino data.

We have presented a general parameterisation of the relevant transition and survival probabilities in the presence of oscillations (within the one-mass scale approximation) and NSI, and we have identified particular combinations of mixing matrix elements $U_{\alpha 4}$ and NSI parameters $\varepsilon_{\alpha\beta}$ entering in the probabilities. This drastically reduces the number of independent parameters and allows us to perform a general fit to global short-baseline data.

We have considered two versions of the (3+1) NSI model. In the general case (denoted NSI^g) we make use of the fact that the neutrino production mechanism in LSND (and in KARMEN) is muon decay (purely leptonic), whereas in all other experiments neutrino production and detection are semi-leptonic, involving transitions between u and d quarks. Therefore, in the presence of suitable NSI parameters we can decouple the transition probabilities in LSND and KARMEN from the rest of the data. In this case we obtain an excellent fit to the global data and the tension between appearance and disappearance experiments is resolved. Let us mention that in this case MiniBooNE does not provide a direct test of LSND, since different combinations of parameters are relevant for them. Also, in the global fit the excess observed in MiniBooNE anti-neutrino data is not reproduced.

For the second version of the (3+1) NSI model we adopt the assumption that NSI involving the charged muon can be neglected. In this case exactly the same NSI parameters are relevant for LSND and KARMEN as for all other experiments. In this constrained model (NSI^c) we make use of the CP violation due to NSI–oscillation interference to reconcile neutrino and anti-neutrino data. We have shown that in the NSI^c model there is a factorisation between appearance and disappearance amplitudes, similar to that in the (3+1) oscillation scheme. Therefore, it is more difficult to satisfy constraints from disappearance experiments and some tension is left in the fit. However, also this model provides significant improvement of the global fit compared to the pure oscillation case.

We have presented the results of our fits in terms of effective parameters, representing the specific combinations of NSI parameters entering in the transition probabilities. However, for both cases, NSI^c and NSI^g, we have provided also examples of how to realise the required parameters in terms of the fundamental mixing and NSI parameters. We have shown that values in safe agreement with bounds on the various ε 's can be found to realise our fits. The examples given in eqs. (25) and (27) require ε 's of order a few $\times 10^{-2}$.

We have compared the quality of the (3+1) NSI fits to an updated fit in the (3+2) oscillation scheme, which also allows for CP violation due to the presence of two relevant

mass scales. Similarly to (3+1) NSI, in (3+2) the appearance experiments can be described very well. However, we confirm previous results that for (3+2) oscillations significant tension remains in the global fit between appearance and disappearance experiments. The improvement of (3+2) compared to (3+1) is not significant, in terms of χ^2 gain per new parameter. Let us mention also that in none of the scenarios considered here we can explain the MiniBooNE low energy excess of events when disappearance data are taken into account. Therefore, we follow the strategy of the MiniBooNE collaboration and exclude the data below 475 MeV from the analysis, relying on a separate explanation for this anomaly.

The predictions of our model for future experiments depend on the detailed realization in terms of mixing and NSI parameters. In general one may expect some signals in searches for deviations from the standard three-flavour oscillation picture in both respects, sterile neutrino oscillations as well as NSI. Several proposals to search for sterile neutrinos at the eV scale have been presented recently, see for example [55–60]. In [61] implications of sterile neutrinos for latest cosmological data have been investigated. Recent studies on NSI in the context of upcoming and far future experiments can be found, e.g., in [62–65].

A specific prediction of our scenario are zero-distance effects in appearance searches [48, 52, 65], since our solutions all include some non-vanishing value of the parameter $|\beta_{\mu e}|$. This parameter induces a non-zero transition probability even at zero distance from the neutrino source, see eq. (11). Hence, the observation of an energy independent appearance probability at very short distances is a characteristic signature from this kind of models. The idea presented in [60] could be particularly useful to search for this effect, since it would allow to map out the E_ν and L dependence of a $\bar{\nu}_e$ appearance signal.

Our model may also provide a signature at the LHC. Typically, realising CC-like interactions as the ones from eq. (1) require a charged particle as mediator. The NSI parameters ε measure the strength of the new interactions relative to the standard weak interaction strength set by G_F . Therefore, from our fit results, $\varepsilon \sim 0.01$, one expects that the mass of a mediator for a dimension-6 operator should be roughly one order of magnitude larger than the W boson mass. Hence, one might expect charged particles to show up at the TeV scale, with good prospects to be observed at LHC. Let us mention, however, that the results of [36, 37] suggest that NSI at the level of 0.01 are difficult to obtain from dimension-6 operators without being in conflict with bounds on charged-lepton processes. As discussed there, a possibility to obtain such large NSI would be to go to dimension-8 operators and allow for some fine tuning.

Acknowledgements

We would like to thank K.S. Babu and W.C. Louis for stimulating discussions and M. Blennow, E. Fernandez-Martinez, and J. Kopp for useful correspondence. We acknowledge the financial support of the European Community under the European Commission Framework Programme 7 Design Study EUROnu, Project Number 212372. The EC is not liable

for any use that may be made of the information contained herein. This work is partly supported by the Transregio Sonderforschungsbereich TR27 “Neutrinos and Beyond” der Deutschen Forschungsgemeinschaft.

Appendix A: $\varepsilon^S \neq \varepsilon^D$ in ν_μ disappearance experiments

As discussed in section II B, the fact that pions couple only to the axial-vector current may lead to the situation that different NSI contribute at neutrino production and detection in ν_μ disappearance experiments. In particular, vector-like NSI, $\varepsilon^{(V)} = \varepsilon^{(R)} + \varepsilon^{(L)}$, will only contribute in the detection process but not at production. This effectively introduces new independent parameters which decouple also the ν_μ disappearance experiments.

Let us introduce the following abbreviations for the various production and detection processes:

$$\begin{aligned}
\mu & : \text{muon decay} \\
\pi & : \text{pion decay} \\
Ne & : \text{neutrino-nucleus CC interaction involving an electron} \\
N\mu & : \text{neutrino-nucleus CC interaction involving a muon}
\end{aligned} \tag{A1}$$

Relaxing now the assumption eq. (15) we have the following set of parameters relevant for the various experiments (in addition to the common Δm_{41}^2):

$$\begin{aligned}
\text{LSND/KARMEN:} & \quad \alpha_{\mu e} = F_{\mu 4}^\mu F_{e 4}^{Ne*}, \quad \beta_{\mu e} = \sum_i F_{\mu i}^\mu F_{e i}^{Ne*} \\
\text{MiniBooNE/NOMAD:} & \quad \alpha_{\mu e} = F_{\mu 4}^\pi F_{e 4}^{Ne*}, \quad \beta_{\mu e} = \sum_i F_{\mu i}^\pi F_{e i}^{Ne*} \\
\text{reactor:} & \quad \alpha_{ee} = |F_{e 4}^{Ne}|^2, \quad \beta_{ee} = 1 \\
\text{CDHS/atmospheric:} & \quad \alpha_{\mu\mu} = F_{\mu 4}^\pi F_{\mu 4}^{N\mu*}, \quad \beta_{\mu\mu} = \sum_i F_{\mu i}^\pi F_{\mu i}^{N\mu*}
\end{aligned} \tag{A2}$$

where the $F_{\alpha i}$ are defined in eq. (7). Now it is possible to have $P_{\mu\mu} = 1$ while allowing for a non-zero transition probability in MiniBooNE, which however, requires some cancellation between NSI parameters and elements of the mixing matrix. For example, one can take

$$F_{\mu 4}^{N\mu} \approx U_{\mu 4}^* + \varepsilon_{\mu s}^{N\mu} U_{\mu s}^* \approx 0, \quad \varepsilon_{\mu s}^\pi \approx 0. \tag{A3}$$

This implies $\alpha_{\mu\mu} \approx 0$ and $\beta_{\mu\mu} \approx 1$ and therefore $P_{\mu\mu} \approx 1$, as required by the data from CDHS and atmospheric neutrinos. On the other hand, $F_{\mu 4}^\pi \approx U_{\mu 4}^*$ and we can have $P_{\mu e} > 0$ for MiniBooNE, including the possibility of CP violation.

The results of such a fit for MiniBooNE are shown as thin-solid (green) histograms in fig. 6, which are qualitatively very similar to our default NSI^g fit. Reactor experiments still constrain the value of $|F_{e 4}^{Ne}|$ to be small, which excludes small values of Δm_{41}^2 where a better fit to the MiniBooNE spectrum would be possible (such as for example for the appearance data only fit shown in fig. 6), and we find $\Delta m_{41}^2 \simeq 0.9 \text{ eV}^2$ at the best fit point. The spectral shape of the signal for such values of Δm_{41}^2 does not allow for a better fit of MiniBooNE data even without the constraint from ν_μ disappearance. Decoupling the ν_μ disappearance data by setting $P_{\mu\mu} = 1$, we find a best fit point with $\chi^2 = 92.7$, to be compared with

95.4 for the standard NSI^g including the assumption eq. (15). Hence, the improvement of the fit by relaxing this assumption is not significant. The reason is that, despite this assumption, there is already very good agreement between appearance and disappearance data, as discussed in section IV. Even with the assumption $\varepsilon^S = \varepsilon^D$ for ν_μ disappearance experiments, the constraints from CDHS and atmospheric data are satisfied in the global fit. Therefore, relaxing this assumption leads only to an insignificant improvement of the fit.

Furthermore, as mentioned above, decoupling ν_μ disappearance data requires some unpleasant cancellation. At the best fit point shown in fig. 6 we find $U_{\mu 4} \approx 0.26$. Therefore, to cancel this in $F_{\mu 4}^{N\mu}$ one needs $\varepsilon_{\mu s}^{N\mu}$ of the same order. Note that the constraints on $\varepsilon_{\mu\alpha}$ at the level of a few percent come from pion decay processes [35], which only apply to axial-vector-like NSI, while here we need vector-like NSI precisely to avoid the contribution to pion decay. Therefore, such large NSI might be phenomenologically viable, though still uncomfortably large. Moreover, there is no reason why they should have values such that they cancel against $U_{\mu 4}$, since these are two unrelated quantities. Hence, together with the observation that the improvement of the fit is not significant, this motivates us to stick in the main text to the assumption eq. (15) in order to simplify the analysis.

Appendix B: MINOS results and NSI

Let us comment briefly on the possibility to apply NSI in source and detector as an explanation for recent MINOS results, which indicate a slight difference between neutrino and anti-neutrino data [47], where we restrict ourselves here to an effective two-flavour framework in the $\mu - \tau$ sector. The mentioned results from MINOS are based on data from ν_μ and $\bar{\nu}_\mu$ disappearance searches. Our formalism allows for CP violation in the survival probability provided NSI are different at neutrino production and detection. Hence, one can use the same mechanism as discussed in appendix A. Since pions couple only to the axial-vector current, vector-like NSI will contribute only at neutrino detection but not at the neutrino source, which is pion decay in MINOS [66]. Note that the one mass scale dominance approximation used in this work applies approximately also for MINOS, though for Δm_{31}^2 . We find that relatively large values of ε are needed, of order 0.1, while at the same time the combined fit of MINOS neutrino and anti-neutrino data does improve only by about 2.5 units in χ^2 .

We have also considered the possibility to use NC-like NSI in the context of MINOS [67–69], which would induce a non-standard matter effect in the $\mu - \tau$ sector, and which therefore could lead to a difference between neutrino and anti-neutrino results. We find that (i) diagonal NSI $\varepsilon_{\mu\mu}^{\text{NC}}, \varepsilon_{\tau\tau}^{\text{NC}} \lesssim 0.5$ have a negligibly small effect on the fit, and (ii) off-diagonal NSI $\varepsilon_{\mu\tau}^{\text{NC}}$ of the order 0.2 lead to an improvement of the combined fit of about 2.5 units in χ^2 . These values for $\varepsilon_{\mu\mu}^{\text{NC}}, \varepsilon_{\mu\tau}^{\text{NC}}, \varepsilon_{\tau\tau}^{\text{NC}}$ are about one order of magnitude larger than the bounds from atmospheric neutrino data [70]. We conclude that neither CC nor NC type

NSI in the $\mu - \tau$ sector provide a viable explanation for a possible deviation of neutrino and anti-neutrino results from present MINOS data. The question whether this conclusions holds also in a more general three-flavour (or maybe four-flavour) framework is left for future work, see also [71, 72].

-
- [1] MiniBooNE, A. A. Aguilar-Arevalo *et al.*, *Observed Event Excess in the MiniBooNE Search for $\bar{\nu}_\mu \rightarrow \bar{\nu}_e$ Oscillations*, (2010), 1007.1150.
 - [2] LSND, A. Aguilar *et al.*, *Evidence for neutrino oscillations from the observation of $\bar{\nu}_e$ appearance in a $\bar{\nu}_\mu$ beam*, Phys. Rev. **D64**, 112007 (2001), hep-ex/0104049.
 - [3] MiniBooNE, A. A. Aguilar-Arevalo *et al.*, *A Search for electron neutrino appearance at the $\Delta m^2 \sim 1eV^2$ scale*, Phys. Rev. Lett. **98**, 231801 (2007), 0704.1500.
 - [4] Y. Declais *et al.*, *Search for neutrino oscillations at 15-meters, 40-meters, and 95-meters from a nuclear power reactor at Bugey*, Nucl. Phys. **B434**, 503 (1995).
 - [5] CHOOZ, M. Apollonio *et al.*, *Search for neutrino oscillations on a long base-line at the CHOOZ nuclear power station*, Eur. Phys. J. **C27**, 331 (2003), hep-ex/0301017.
 - [6] F. Dydak *et al.*, *A Search for Muon-neutrino Oscillations in the Δm^2 Range $0.3 eV^2$ to $90 eV^2$* , Phys. Lett. **B134**, 281 (1984).
 - [7] MiniBooNE, A. A. Aguilar-Arevalo *et al.*, *A search for muon neutrino and antineutrino disappearance in MiniBooNE*, Phys. Rev. Lett. **103**, 061802 (2009), 0903.2465.
 - [8] Super-Kamiokande, Y. Ashie *et al.*, *A Measurement of Atmospheric Neutrino Oscillation Parameters by Super-Kamiokande I*, Phys. Rev. **D71**, 112005 (2005), hep-ex/0501064.
 - [9] S. M. Bilenky, C. Giunti, W. Grimus, and T. Schwetz, *Four-neutrino mass spectra and the Super-Kamiokande atmospheric up-down asymmetry*, Phys. Rev. **D60**, 073007 (1999), hep-ph/9903454.
 - [10] J. T. Peltoniemi and J. W. F. Valle, *Reconciling dark matter, solar and atmospheric neutrinos*, Nucl. Phys. **B406**, 409 (1993), hep-ph/9302316.
 - [11] J. T. Peltoniemi, D. Tommasini, and J. W. F. Valle, *Reconciling dark matter and solar neutrinos*, Phys. Lett. **B298**, 383 (1993).
 - [12] D. O. Caldwell and R. N. Mohapatra, *Neutrino mass explanations of solar and atmospheric neutrino deficits and hot dark matter*, Phys. Rev. **D48**, 3259 (1993).
 - [13] A. Strumia, *Interpreting the LSND anomaly: sterile neutrinos or CPT-violation or...?*, Phys. Lett. **B539**, 91 (2002), hep-ph/0201134.
 - [14] M. Maltoni, T. Schwetz, M. A. Tortola, and J. W. F. Valle, *Ruling out four-neutrino oscillation interpretations of the LSND anomaly?*, Nucl. Phys. **B643**, 321 (2002), hep-ph/0207157.
 - [15] O. L. G. Peres and A. Y. Smirnov, *(3+1) spectrum of neutrino masses: A chance for LSND?*, Nucl. Phys. **B599**, 3 (2001), hep-ph/0011054.
 - [16] M. Sorel, J. M. Conrad, and M. Shaevitz, *A combined analysis of short-baseline neutrino*

- experiments in the (3+1) and (3+2) sterile neutrino oscillation hypotheses*, Phys. Rev. **D70**, 073004 (2004), hep-ph/0305255.
- [17] G. Karagiorgi *et al.*, *Leptonic CP violation studies at MiniBooNE in the (3+2) sterile neutrino oscillation hypothesis*, Phys. Rev. **D75**, 013011 (2007), hep-ph/0609177.
- [18] M. Maltoni and T. Schwetz, *Sterile neutrino oscillations after first MiniBooNE results*, Phys. Rev. **D76**, 093005 (2007), 0705.0107.
- [19] G. Karagiorgi, Z. Djurcic, J. M. Conrad, M. H. Shaevitz, and M. Sorel, *Viability of $\Delta m^2 \sim 1 eV^2$ sterile neutrino mixing models in light of MiniBooNE electron neutrino and antineutrino data from the Booster and NuMI beamlines*, Phys. Rev. **D80**, 073001 (2009), 0906.1997.
- [20] E. Ma, G. Rajasekaran, and I. Stancu, *Hierarchical four-neutrino oscillations with a decay option*, Phys. Rev. **D61**, 071302 (2000), hep-ph/9908489.
- [21] S. Palomares-Ruiz, S. Pascoli, and T. Schwetz, *Explaining LSND by a decaying sterile neutrino*, JHEP **09**, 048 (2005), hep-ph/0505216.
- [22] H. Murayama and T. Yanagida, *LSND, SN1987A, and CPT violation*, Phys. Lett. **B520**, 263 (2001), hep-ph/0010178.
- [23] G. Barenboim, L. Borissov, and J. D. Lykken, *CPT violating neutrinos in the light of KamLAND*, (2002), hep-ph/0212116.
- [24] M. C. Gonzalez-Garcia, M. Maltoni, and T. Schwetz, *Status of the CPT violating interpretations of the LSND signal*, Phys. Rev. **D68**, 053007 (2003), hep-ph/0306226.
- [25] V. Barger, D. Marfatia, and K. Whisnant, *LSND anomaly from CPT violation in four-neutrino models*, Phys. Lett. **B576**, 303 (2003), hep-ph/0308299.
- [26] V. A. Kostelecky and M. Mewes, *Lorentz violation and short-baseline neutrino experiments*, Phys. Rev. **D70**, 076002 (2004), hep-ph/0406255.
- [27] A. de Gouvea and Y. Grossman, *A three-flavor, Lorentz-violating solution to the LSND anomaly*, Phys. Rev. **D74**, 093008 (2006), hep-ph/0602237.
- [28] T. Katori, V. A. Kostelecky, and R. Tayloe, *Global three-parameter model for neutrino oscillations using Lorentz violation*, Phys. Rev. **D74**, 105009 (2006), hep-ph/0606154.
- [29] G. Barenboim and N. E. Mavromatos, *CPT violating decoherence and LSND: A possible window to Planck scale physics*, JHEP **01**, 034 (2005), hep-ph/0404014.
- [30] Y. Farzan, T. Schwetz, and A. Y. Smirnov, *Reconciling results of LSND, MiniBooNE and other experiments with soft decoherence*, JHEP **07**, 067 (2008), 0805.2098.
- [31] D. B. Kaplan, A. E. Nelson, and N. Weiner, *Neutrino oscillations as a probe of dark energy*, Phys. Rev. Lett. **93**, 091801 (2004), hep-ph/0401099.
- [32] V. Barger, D. Marfatia, and K. Whisnant, *Confronting mass-varying neutrinos with MiniBooNE*, Phys. Rev. **D73**, 013005 (2006), hep-ph/0509163.
- [33] H. Pas, S. Pakvasa, and T. J. Weiler, *Sterile - active neutrino oscillations and shortcuts in the extra dimension*, Phys. Rev. **D72**, 095017 (2005), hep-ph/0504096.
- [34] T. Schwetz, *LSND versus MiniBooNE: Sterile neutrinos with energy dependent masses and mixing?*, JHEP **02**, 011 (2008), 0710.2985.

- [35] C. Biggio, M. Blennow, and E. Fernandez-Martinez, *General bounds on non-standard neutrino interactions*, JHEP **08**, 090 (2009), 0907.0097.
- [36] S. Antusch, J. P. Baumann, and E. Fernandez-Martinez, *Non-Standard Neutrino Interactions with Matter from Physics Beyond the Standard Model*, Nucl. Phys. **B810**, 369 (2009), 0807.1003.
- [37] M. B. Gavela, D. Hernandez, T. Ota, and W. Winter, *Large gauge invariant non-standard neutrino interactions*, Phys. Rev. **D79**, 013007 (2009), 0809.3451.
- [38] Y. Grossman, *Nonstandard neutrino interactions and neutrino oscillation experiments*, Phys. Lett. **B359**, 141 (1995), hep-ph/9507344.
- [39] M. C. Gonzalez-Garcia, Y. Grossman, A. Gusso, and Y. Nir, *New CP violation in neutrino oscillations*, Phys. Rev. **D64**, 096006 (2001), hep-ph/0105159.
- [40] P. Huber, T. Schwetz, and J. W. F. Valle, *Confusing non-standard neutrino interactions with oscillations at a neutrino factory*, Phys. Rev. **D66**, 013006 (2002), hep-ph/0202048.
- [41] D. Meloni, T. Ohlsson, and H. Zhang, *Exact and Approximate Formulas for Neutrino Mixing and Oscillations with Non-Standard Interactions*, JHEP **04**, 033 (2009), 0901.1784.
- [42] S. Bergmann and Y. Grossman, *Can lepton flavor violating interactions explain the LSND results?*, Phys. Rev. **D59**, 093005 (1999), hep-ph/9809524.
- [43] S. Bergmann, H. V. Klapdor-Kleingrothaus, and H. Pas, *Lepton number violation interactions and their effects on neutrino oscillation experiments*, Phys. Rev. **D62**, 113002 (2000), hep-ph/0004048.
- [44] K. S. Babu and S. Pakvasa, *Lepton number violating muon decay and the LSND neutrino anomaly*, (2002), hep-ph/0204236.
- [45] K. M. Zurek, *New matter effects in neutrino oscillation experiments*, JHEP **10**, 058 (2004), hep-ph/0405141.
- [46] A. E. Nelson and J. Walsh, *Short Baseline Neutrino Oscillations and a New Light Gauge Boson*, Phys. Rev. **D77**, 033001 (2008), 0711.1363.
- [47] MINOS, P. Vahle, talk at the 24th International Conference On Neutrino Physics And Astrophysics (Neutrino 2010), June 14, 2010 (Athens, Greece).
- [48] E. Fernandez-Martinez, M. B. Gavela, J. Lopez-Pavon, and O. Yasuda, *CP-violation from non-unitary leptonic mixing*, Phys. Lett. **B649**, 427 (2007), hep-ph/0703098.
- [49] KARMEN, B. Armbruster *et al.*, *Upper limits for neutrino oscillations muon-antineutrino to electron-antineutrino from muon decay at rest*, Phys. Rev. **D65**, 112001 (2002), hep-ex/0203021.
- [50] F. Boehm *et al.*, *Final results from the Palo Verde Neutrino Oscillation Experiment*, Phys. Rev. **D64**, 112001 (2001), hep-ex/0107009.
- [51] NOMAD, P. Astier *et al.*, *Search for $\nu_\mu \rightarrow \nu_e$ oscillations in the NOMAD experiment*, Phys. Lett. **B570**, 19 (2003), hep-ex/0306037.
- [52] P. Langacker and D. London, *Lepton number violation and massless nonorthogonal neutrinos*, Phys. Rev. **D38**, 907 (1988).

- [53] S. M. Bilenky, C. Giunti, and W. Grimus, *Neutrino mass spectrum from the results of neutrino oscillation experiments*, Eur. Phys. J. **C1**, 247 (1998), hep-ph/9607372.
- [54] M. Maltoni and T. Schwetz, *Testing the statistical compatibility of independent data sets*, Phys. Rev. **D68**, 033020 (2003), hep-ph/0304176.
- [55] A. Donini, K.-i. Fuki, J. Lopez-Pavon, D. Meloni, and O. Yasuda, *The discovery channel at the Neutrino Factory: $\nu_\mu \rightarrow \nu_\tau$ pointing to sterile neutrinos*, JHEP **08**, 041 (2009), 0812.3703.
- [56] C. Giunti, M. Laveder, and W. Winter, *Short-Baseline Electron Neutrino Disappearance at a Neutrino Factory*, Phys. Rev. **D80**, 073005 (2009), 0907.5487.
- [57] B. Baibussinov *et al.*, *A new search for anomalous neutrino oscillations at the CERN-PS*, (2009), 0909.0355.
- [58] S. K. Agarwalla, P. Huber, and J. M. Link, *Constraining sterile neutrinos with a low energy beta- beam*, JHEP **01**, 071 (2010), 0907.3145.
- [59] D. Meloni, J. Tang, and W. Winter, *Sterile neutrinos beyond LSND at the Neutrino Factory*, (2010), 1007.2419.
- [60] S. K. Agarwalla and P. Huber, *LSND reloaded*, (2010), 1007.3228.
- [61] J. Hamann, S. Hannestad, G. G. Raffelt, I. Tamborra, and Y. Y. Y. Wong, *Cosmology seeking friendship with sterile neutrinos*, (2010), 1006.5276.
- [62] J. Kopp, M. Lindner, T. Ota, and J. Sato, *Non-standard neutrino interactions in reactor and superbeam experiments*, Phys. Rev. **D77**, 013007 (2008), 0708.0152.
- [63] T. Ohlsson and H. Zhang, *Non-Standard Interaction Effects at Reactor Neutrino Experiments*, Phys. Lett. **B671**, 99 (2009), 0809.4835.
- [64] J. Kopp, T. Ota, and W. Winter, *Neutrino factory optimization for non-standard interactions*, Phys. Rev. **D78**, 053007 (2008), 0804.2261.
- [65] D. Meloni, T. Ohlsson, W. Winter, and H. Zhang, *Non-standard interactions versus non-unitary lepton flavor mixing at a neutrino factory*, JHEP **04**, 041 (2010), 0912.2735.
- [66] J. Kopp, P. A. N. Machado, and S. J. Parke, *to appear*, (2010).
- [67] N. Engelhardt, A. E. Nelson, and J. R. Walsh, *Apparent CPT Violation in Neutrino Oscillation Experiments*, Phys. Rev. **D81**, 113001 (2010), 1002.4452.
- [68] W. A. Mann, D. Cherdack, W. Musial, and T. Kafka, *Apparent multiple Δm_{32}^2 in muon anti-neutrino and muon neutrino survival oscillations from non-standard interaction matter effect*, (2010), 1006.5720.
- [69] J. Heeck and W. Rodejohann, *Gauged $L_\mu - L_\tau$ and different Muon Neutrino and Anti-Neutrino Oscillations: MINOS and beyond*, (2010), 1007.2655.
- [70] M. C. Gonzalez-Garcia and M. Maltoni, *Atmospheric neutrino oscillations and new physics*, Phys. Rev. **D70**, 033010 (2004), hep-ph/0404085.
- [71] A. Friedland and C. Lunardini, *Two modes of searching for new neutrino interactions at MINOS*, Phys. Rev. **D74**, 033012 (2006), hep-ph/0606101.
- [72] M. Blennow, T. Ohlsson, and J. Skrotzki, *Effects of non-standard interactions in the MINOS experiment*, Phys. Lett. **B660**, 522 (2008), hep-ph/0702059.